



CrossMark
click for updates

Cite this: *Lab Chip*, 2015, 15, 1205

Application of multiple levels of fluid shear stress to endothelial cells plated on polyacrylamide gels†

P. A. Galie,^{ab} A. van Oosten,^{ab} C. S. Chen^c and P. A. Janmey^{*ab}

Measurements of endothelial cell response to fluid shear stress have previously been performed on unphysiologically rigid substrates. We describe the design and implementation of a microfluidic device that applies discrete levels of shear stress to cells plated on hydrogel-based substrates of physiologically-relevant stiffness. The setup allows for measurements of cell morphology and inflammatory response to the combined stimuli, and identifies mechanisms by which vascular stiffening leads to pathological responses to blood flow. We found that the magnitude of shear stress required to affect endothelial cell morphology and inflammatory response depended on substrate stiffness. Endothelial cells on 100 Pa substrates demonstrate a greater increase in cell area and cortical stiffness and decrease in NF- κ B nuclear translocation in response to TNF- α treatment compared to controls than cells plated on 10 kPa substrates. The response of endothelial cells on soft substrates to shear stress depends on the presence of hyaluronan (HA). These results emphasize the importance of substrate stiffness on endothelial function, and elucidate a means by which vascular stiffening in aging and disease can impact the endothelium.

Received 17th October 2014,
Accepted 31st December 2014

DOI: 10.1039/c4lc01236d

www.rsc.org/loc

Introduction

Both aging and multiple cardiovascular pathologies including atherosclerosis, diabetes, and hypertriglyceridemia are characterized by a stiffening of the vascular wall.^{1–3} The shear modulus (calculated from its measured Young's modulus) at the arterial surface in mice increases from less than 1600 Pa in healthy wild type mice to >3300 Pa in apoE^{−/−} mice⁴ or after mechanical injury to wt mice,⁵ and rises even farther to >13 kPa during atherosclerosis.⁴ Protein deposition and remodelling decrease the compliance of the extracellular matrix on the basal side of the endothelium, and the response of endothelial cells to vascular stiffening can have negative consequences on endothelial cell function and survival.⁶ However, the effect of increased stiffness on the response of endothelial cells to fluid shear stress is relatively understudied. Previously, substrate mechanics and shear stress have been studied *in vitro* separately: either by changing substrate stiffness in static conditions, or by applying shear to cells plated on glass or plastic. The present study uses a novel microfluidic device to investigate how the combination of these mechanical stimuli affects the inflammatory

response of endothelial cells, which is a crucial component of cardiovascular disease.

Several landmark studies have established the role of substrate mechanics in determining cell behavior.^{7–9} Specifically, much has been done to analyze the response of the endothelium to varying substrate stiffness. Endothelial cells cultured on stiff substrates were found to exhibit higher elastic moduli.¹⁰ Morphology and migration were also shown to be dependent on the stiffness of the substrate upon which endothelial cells were plated.^{11–13} Substrate stiffness can affect inflammatory responses of endothelial cells *in vitro*.¹⁴ Additionally, the role of extracellular matrix mechanics in inflammation is being increasingly understood *in vivo*.¹⁵ A causal relationship between inflammation and arterial stiffness has been established clinically,^{16,17} and it is possible that arterial stiffness affects inflammation in a feedback mechanism.

In addition to substrate mechanics, endothelial cells are also known to be sensitive to fluid flow. Early studies demonstrated the ability of fluid flow to dictate the morphology and migration of endothelial cells.¹⁸ Exposing endothelial cells in culture to shear stress has also been associated with modulation of the inflammatory response.^{19–21} Endothelial cells exposed to a 1.2 Pa level of shear stress modulated their response to the inflammatory cytokine TNF- α , as measured by nuclear localization of NF- κ B.²² Although most *in vitro* studies investigate shear stress on cells plated on unphysiologically rigid substrates, there have been exceptions.

^a Dept of Physiology, University of Pennsylvania, Philadelphia, PA, USA.

E-mail: janmey@mail.med.upenn.edu

^b Dept of Bioengineering, University of Pennsylvania, Philadelphia, PA, USA

^c Dept of Bioengineering, Boston University, Boston, MA, USA

† Electronic supplementary information (ESI) available: Photomasks for fabrication of the step device. See DOI: 10.1039/c4lc01236d

A study demonstrating that shear stress increases traction force exerted by endothelial cells used a polyacrylamide (PAA) gel of 28 kPa elastic modulus.²³ Endothelial cells have also been exposed to shear stress on flexible micropost arrays.^{24–26}

In the present study we sought to determine how the combined effects of substrate mechanics and fluid shear stress modulate the mechano-sensing response of endothelial cells. A microfluidic apparatus able to vary shear stress in discrete steps on substrates with several magnitudes of stiffness is used for this purpose. In addition to studying morphological changes, we investigate the effect of the combined mechanical stimuli on the inflammatory response of the endothelial cells.

Experimental

Fabrication

We polymerized PAA gels on silanized glass coverslips treated for 30 minutes with 0.5% glutaraldehyde by combining volumes of acrylamide, bis-acrylamide, tetramethylethylenediamine (TEMED), and ammonium persulfate (APS). To create 100 Pa, 2.5 kPa, 3 kPa, 10 kPa, and 30 kPa gels we combined acrylamide with bis-acrylamide; at ratios of 3, 0.06%; 7.5, 0.075%; 7.5, 0.1%; 12, 0.15%; and 12, 0.28% respectively. We quantified gel stiffness using atomic force microscopy to verify elastic modulus using methods described in detail elsewhere.⁹ For cell morphology experiments, we produced three sets of gels with a range of shear elastic moduli beyond what is normally found in human vasculature: 10 kPa, 2.5 kPa, and 100 Pa. For inflammatory response experiments, 3 kPa and 30 kPa gels were used to mimic healthy and diseased vasculature, respectively. After polymerization, we treated gels with 0.1 mM sulfo-SANPAH and UV-treated for 8 minutes. Gels were then incubated with 0.1 mg mL⁻¹ fibronectin at 4 °C overnight, and stored in PBS prior to attachment with the flow gasket. Gels were used within 2 weeks of polymerization. We used silicon masters to cast polydimethylsiloxane (PDMS) gaskets. Briefly, we spun SU-8 photoresist on silicon wafers to create 100 µm thick layers that were successively etched using photolithography and developed with propylene glycol methyl ether acetate (PGMEA) to create the step pattern of the device. The resulting silicon master was used to mold a negative PDMS stamp that we then used to create the PDMS gaskets. Baking at 130 °C for only five minutes partially polymerizes the gasket, which helps adhere the gasket to the coverslip. The gasket and coverslip/gel are pressed together manually, and baked for 45 minutes at 55 °C in 100% humidity to facilitate attachment and complete polymerization of the gasket while preventing drying of the gel. An illustration of the device construction can be found in Fig. 1.

Computational fluid dynamics

To determine the shear stress distribution on the surface of the PAA gel during application of flow, we imported and discretized the fluid volume within the device in a

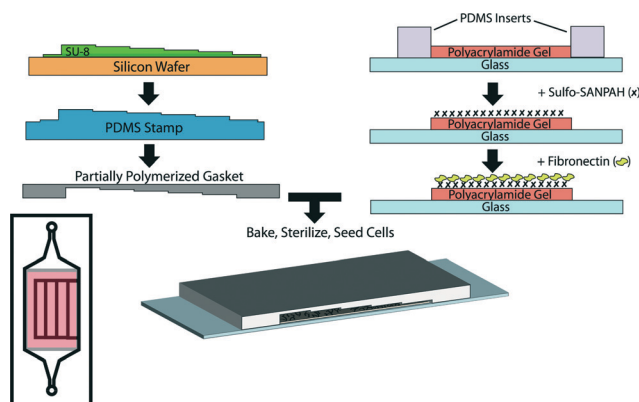


Fig. 1 Device manufacture and preparation: the PDMS step gasket is constructed using traditional soft lithography techniques and then adhered to a coverslip containing a 100 nm height, rectangular-shaped polyacrylamide gel coated with fibronectin. Flow is applied through the device using a peristaltic pump connected to the inlet and outlet ports of the device.

commercial finite element code (COMSOL). We refined the mesh along the boundaries of the device to resolve the boundary layer of the viscous flow. We used the steady Navier–Stokes equation to describe flow within the device:

$$\rho(\mathbf{v} \cdot \nabla \mathbf{v}) = -\nabla p + \mu \nabla^2 \mathbf{v} \quad (1)$$

where ρ is density, \mathbf{v} is velocity, p is pressure, and μ is dynamic viscosity. The momentum term of the equation, represented by the dot product of velocity with its tensor derivative, is included because the maximum Reynolds number of the flow is approximately 25, rendering Stokes law insufficient to describe the flow. For example, the corners of the steps create small vortices in the flow at the entrance of the steps. These secondary flows could not be predicted by Stokes flow. We used a velocity boundary condition at the inlet, calculated from the imposed flow rate of the pump and the cross-sectional area of the device. We set the exit boundary to zero pressure, since the outlet of the device was open to the atmosphere. The walls of the device were given the no-slip condition of zero velocity at the wall surface. The viscosity of the dextran-containing medium was measured at shear rates in the range of those occurring in the flow device using a Bohlin rheometer at 37 °C. Results of the computational model can be found in Fig. 2A–B.

Particle image velocimetry

In order to validate the computational model, we measured the velocity of 3 µm fluorescent beads within the dextran-containing medium by time-lapse video microscopy. The velocity of the beads were low enough that a 5 ms exposure was sufficient to track their velocities. We used a bead concentration of 1 wt% to assure individual beads could be tracked. The maximum velocity within each step occurs at the midpoint of the step height, so we focused the microscope at the midpoint of the height of each channel and

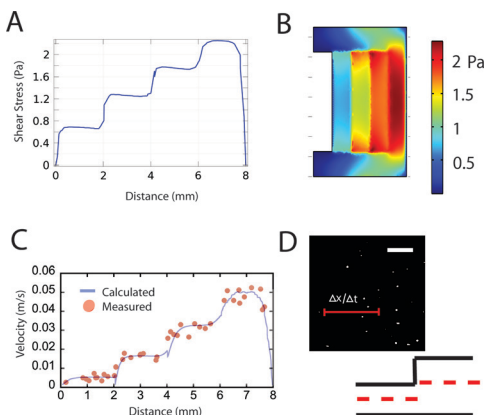


Fig. 2 A) Estimated wall shear stress along the centerline of the step device using the finite element model. B) Accompanying wall shear stress contour. C) Comparison of measured particle velocity and velocity magnitude predicted by the finite element model. D) Schematic of the validation approach: particles were measured at the half-height of each step (scale bar = 50 μm).

measured the distance travelled by each bead in that focal plane; out-of-focus beads were not counted. The velocity of the bead as well as its position from the edge of the step were recorded and graphed against the predicted velocity from the simulation. The results of the velocimetry and comparison to the finite element model can be found in Fig. 2C–D.

Cell culture and seeding

Bovine aorta endothelial cells (BAECs) of passage 6 through 10 obtained from Clonetics were cultured in DMEM supplemented with 10% FBS and 1% penicillin/streptomycin. Cells were trypsinized and resuspended at a density of 10 million cells mL^{-1} and perfused into the device. The cells were allowed to attach for one hour prior to flow. During cell attachment, the device was periodically tilted to assure even seeding across the gel despite the varying heights. We then applied recirculating flow of medium containing dextran with a variable-speed rotary peristaltic pump. Flow freely exited the device into a 100 mm petri dish that was fitted with a tube returning flow to the pump. We applied flow for 24 hours for morphology experiments and 5 and 24 hours for the inflammatory response experiments. For the TNF-alpha studies, human umbilical cord endothelial cells (HUVECs) obtained from Lonza were used for the experiments instead of BAECs, since BAECs would not respond to the human-derived TNF-alpha. HUVECs were cultured in EGM-2 culture medium and used between passages 6 and 8. For experiments involving hyaluronidase treatment, after one hour of attachment, we replaced the culture medium with serum-free medium containing hyaluronidase and incubated for three hours prior to application of flow. This process was repeated with the HA synthase inhibitor, 4-methylumbelliferone (4-MU), with the exception of the use of serum-free medium. Also in contrast to the hyaluronidase experiments, 4-MU was added to the perfusing medium for the entirety of the experiment.

Immunofluorescence

Cells were fixed using 3.7% paraformaldehyde for 10 minutes at room temperature, and the PDMS gasket was removed from the glass coverslip to fully expose the cells. 0.1% Triton X-100 was used to permeabilize the cells for 30 minutes at 37 °C. For morphology experiments, BAECs were stained with Texas Red-phalloidin (1:100) and DAPI (1:1000) at 37 °C for one hour and visualized on a Leica fluorescent microscope at 10 \times magnification. For the TNF-alpha experiments, cells were fixed and permeabilized in the same manner. Cells were stained with a rabbit polyclonal antibody against NF- κ B (1:500) overnight at 4 °C, washed thoroughly with PBS, and stained with a Texas Red-conjugated secondary antibody (1:1000) and DAPI (1:1000) for 45 minutes at 37 °C. Nuclear localization was quantified as a 50% greater intensity in the nucleus compared to the cytoplasm.

Atomic force microscopy

After applying fluid shear for 24 hours, we removed the top gasket of the device and added PBS to the cells to prevent drying. A silicon-nitride tip fitted with a 3 μm bead was used to indent cells up to 2 μm at a fixed frequency of 1 Hz. Resulting force/displacement curves were fitted to a Hertz model to estimate the elastic modulus of the cells. For each cell, we averaged three measurements taken at different locations in the region between the nucleus and the periphery. For each experimental condition, at least five cells were measured and averaged.

TNF-alpha response

After 5 hours of shear application, we removed the top gasket of the device and washed the cells with PBS. We then incubated cells with 20 ng mL^{-1} TNF- α in PBS at 37 °C for 15 minutes. Following the incubation, cells were fixed and prepared for immunofluorescence.

Statistical analysis

For analysis of the effect of fluid shear stress, analysis of variances (ANOVAs) and post-hoc Tukey's multiple comparison tests ($P < .05$) were used to compare multiple groups. A Student's t test was used for pairwise comparisons of data sets.

Results

Previous studies have shown that a fluid shear stress magnitude of approximately 0.3 Pa²⁷ is required to align subconfluent endothelial cells with the direction of flow on plastic substrates. Shear stress *in vivo* varies between 1 and 2 Pa in large vessels and 4 and 5 Pa in capillaries.²⁸ As shown in Fig. 3, a shear stress of 0.6 Pa aligned cells on the 10 kPa gel, in agreement with the previous literature. However, as gel stiffness decreased in magnitude, larger levels of shear stress were required to align the subconfluent endothelial

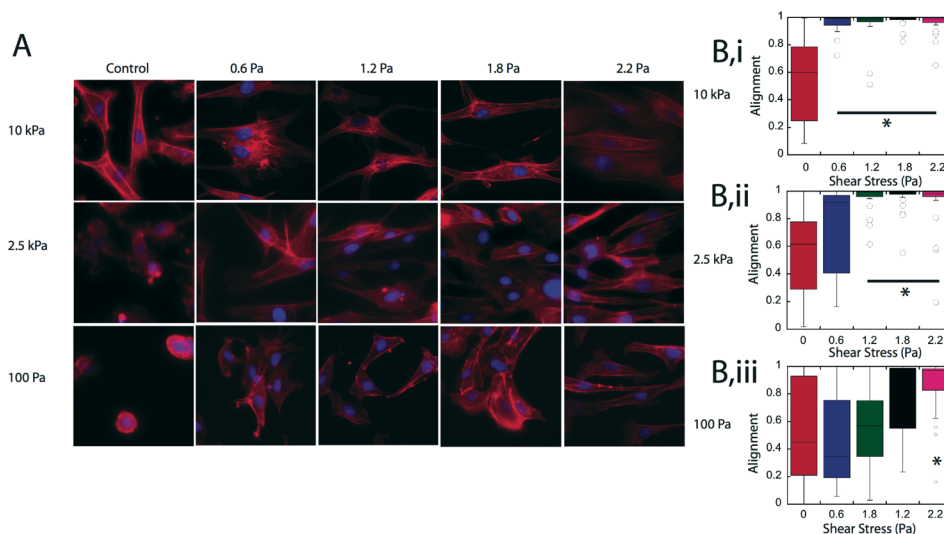


Fig. 3 A) Phalloidin and DAPI stains of BAECs plated on three levels of substrate stiffness and exposed to static control and four levels of shear stress for 24 hours (each image is $75 \times 75 \mu\text{m}$). B) Alignment of cells on 10 kPa (B,i), 2.5 kPa (B,ii), and 100 Pa (B,iii) substrate stiffness, * denotes $p < 0.05$ when compared to static controls using Tukey multiple comparison tests. The data was produced over 3 independent experiments, and 25–30 individual cells were measured for each stiffness and shear condition.

cells, indicating an effect of substrate stiffness on cell response to fluid shear stress.

To further explore this effect, cells plated on three levels of substrate stiffness (100 Pa, 2.5 kPa, and 10 kPa) were exposed to discrete levels of shear stress and stained with phalloidin and DAPI to elucidate their morphology in response to the combined mechanical stimuli. Fig. 3 summarizes the results of these experiments. On the 10 kPa substrate, increasing shear stress from 0 to 2.2 Pa did not have a drastic effect on cell morphology relative to the softer substrates. In contrast, on the 100 Pa substrate, cells appeared spherical and did not spread in the absence of fluid flow. However, addition of 0.6 Pa shear stress was sufficient to induce a spreading response, and further increasing the shear to 2.2 Pa had a pronounced effect on cell shape.

Fig. 3B quantifies the alignment of cells exposed to the same substrate stiffness and shear stress combinations. Alignment was quantified by dividing the dot product of the long axis of the cell and the direction of flow by the magnitude of these vectors to create a normalized quantity (parallel = 1, perpendicular = 0). Fig. 3B,i shows alignment data for the 10 kPa substrate. At all levels of applied shear (0.6–2.2 Pa), the distributions demonstrated significant alignment compared to the static control. On the 2.5 kPa substrates, 1.2 Pa shear stress was required to align the cells, evidenced by the random distributions of cell axis at static and 0.6 Pa shear levels. On 100 Pa stiffness, the effect is even more pronounced: cells don't exhibit significant alignment until exposure to 2.2 Pa of shear stress. Taken together, these results demonstrate that cell alignment in response to shear stress significantly depends on the stiffness of the substrate.

In addition to quantifying cell alignment, the images in Fig. 3 were also used to determine the cell area response. Moreover, AFM measurements were used to determine if the

cortical stiffness of the cells followed the same trend as cell area. Fig. 4 shows the cell areas and elastic moduli for cells exposed to the aforementioned range of substrate stiffness and shear stress conditions. On 10 kPa gels, there was no significant increase in cell area over the range of shear stresses applied, but cells exposed to 1.8 Pa of shear stress exhibited significantly augmented elastic modulus. At 2.5 kPa, the cell area significantly increased only in response

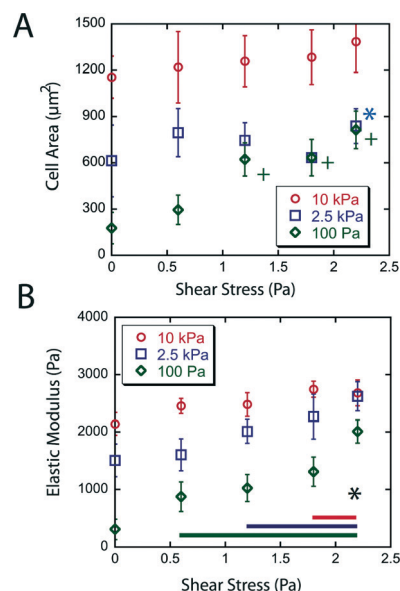


Fig. 4 A) Cell areas and B) elastic moduli of BAECs exposed to varying shear stress and substrate stiffness. * and + denote significance compared to the static control for each substrate stiffness. Data for cell area was produced in parallel with the alignment data (3 independent experiments and $25 < n < 30$). For cell elastic moduli, data was produced using 1 independent experiment and $3 < n < 15$.

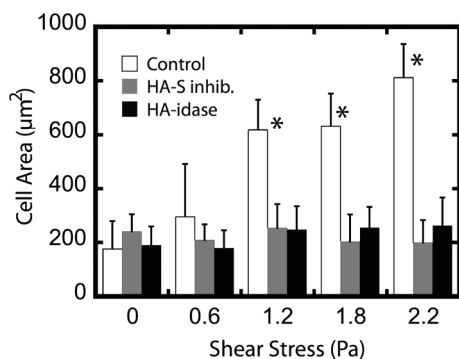


Fig. 5 Cell area of BAECs plated on 100 Pa and exposed to shear stress untreated (control), pre-treated for 3 hours with hyaluronidase (HA-idase), or treated with an HA synthase inhibitor (4-MU). Data was produced using 2 individual experiments for each treatment and $28 < n < 32$.

to 2.2 Pa shear, but the elastic modulus was significantly higher after only 1.2 Pa of shear. Hence, on both 10 kPa and 2.5 kPa gels, the changes in cell stiffness did not mirror the trends in cell area. However, on 100 Pa, both the cell area and cortical stiffness significantly increased with application of fluid shear stress of 0.6 Pa and higher.

In static conditions, the elastic moduli of cells plated on the 2.5 kPa were greater than those of cells on 100 Pa, consistent with previously reported stiffness-sensing behaviour. However, the application of 2.2 Pa of shear stress produced statistically similar elastic moduli between cells on 2.5 kPa and 100 Pa substrates, indicating that shear stress could override the response of the endothelial cells to substrate stiffness. Nonetheless, for all levels of shear stress, the cell area and elastic modulus of cells plated on the 100 Pa were significantly less than cells on the 10 kPa gel, indicating a limit to which shear stress could overcome the effect of substrate stiffness.

We next investigated the mechanism by which the subconfluent endothelial cells responded to the applied shear stress while adhered to the polyacrylamide gels. Because the cells lack the cell-cell junctions present in a confluent monolayer, we did not pursue the well-established PECAM-VE-cadherin-VEGFR2 mechanotransduction pathway. Rather, we focused on hyaluronan, an integral component of the endothelial glycocalyx. The glycocalyx has previously been identified as a sensor of shear stress.^{29,30} One of hyaluronan's cell surface receptors, cd44, is upstream of the Rho/ROCK pathway, and hyaluronan has previously been associated with spreading on soft substrates.³¹ Therefore, cells on the 100 Pa substrates were exposed to hyaluronidase, an enzyme that degrades this glycosaminoglycan, and 4-methylumbelliferone (4-MU), a hyaluronan synthase inhibitor, to determine if hyaluronan was required for spreading in response to shear stress. Fig. 5 indicates that both degrading the existing hyaluronan with hyaluronidase and inhibiting the production of HA with 4-MU did not affect the adherent area of the cells in the absence of flow, but both agents effectively blocked the spreading response on soft substrates over the observed time period. Even at the highest applied level of shear stress, 2.2 Pa, no significant increase in spreading was observed in the treated cells. The results suggest that hyaluronan is a necessary component of the shear sensing mechanism of cells on soft substrates.

Having demonstrated the effect of substrate stiffness on the stiffness and morphology of endothelial cells exposed to shear stress, we next investigated their inflammatory response. Using a short period of flow stimulation similar to the hyaluronan experiments, cells were sheared and then exposed to 20 ng mL⁻¹ TNF- α for 15 minutes, followed by fixation with paraformaldehyde. As Fig. 6 illustrates, cells

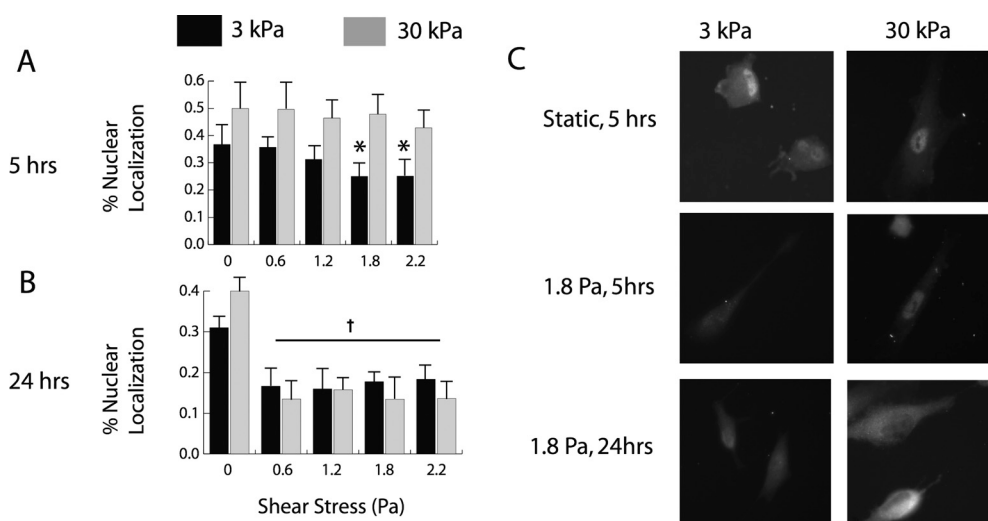


Fig. 6 A) Measurement of NF- κ B translocation to the nucleus in response to 20 ng mL⁻¹ TNF- α post shearing for 5 hours. A significant decrease in nuclear translocation was only observed in cells plated on the 3 kPa substrates (* denotes $p < 0.05$ compared to static controls). B) NF- κ B translocation after 24 hours of flow (\dagger denotes $p < 0.05$ compared to static controls). C) Images of cells exposed to static or 1.8 Pa for 5 and 24 hours on the two levels of substrate stiffness. Images are $40 \times 40 \mu\text{m}$. Data was generated with 4 separate experiments and $22 < n < 36$.

plated on 30 kPa PAA gels exhibited a higher sensitivity to TNF- α treatment than cells on 3 kPa gels after 5 hours of flow, quantified by translocation of NF- κ B to the nucleus (Fig. 6A). The static control indicates a baseline increase caused solely by substrate mechanics. Interestingly, on the 30 kPa substrates, application of shear did not significantly decrease the number of cells positive for nuclear localization of NF- κ B. In contrast, on 3 kPa substrates, cells exhibited a significant decrease in NF- κ B localization to the nucleus in response to increasing levels of fluid shear stress. This result mirrors the morphological data: substrate stiffness masks the cell response to the applied range of fluid shear stress. However, after applying flow for 24 hours and then treating with TNF- α , there was no significant difference in the inflammatory response of cells plated on 3 or 30 kPa substrates (Fig. 6B). This result implies that at the 24 hour time scale laminar flow is sufficiently atheroprotective to mute the effect of substrate stiffness.

To determine if hyaluronan also plays a role in the modulation of the inflammatory response of sheared endothelial cells, the TNF- α experiment was repeated with hyaluronidase-treated cells. Fig. 7 demonstrates that disrupting hyaluronan in static cultures did not change the increased response to TNF- α of HUVECs on stiff substrates, but eliminated the modest decrease in NF- κ B localization in HUVECs on soft substrates with increased shear stress. This result provides additional evidence that hyaluronan is important for shear sensing on soft substrates. Because substrate stiffness increased the inflammatory response, cells were also treated with 10 μ M y27632, a competitive inhibitor of p160ROCK and ROCK II.

As Fig. 7 shows, y27 blocked the stiffness-induced increase in NF- κ B nuclear localization on the 30 kPa substrate. More interestingly, y27 inhibited the flow-induced decrease in NF- κ B nuclear localization on both the 3 kPa and 30 kPa substrates. This result suggests that the mechanotransduction of fluid flow and substrate stiffness share a ROCK-associated pathway, and could potentially explain the saturation effect of substrate stiffness on the cell response to fluid shear stress.

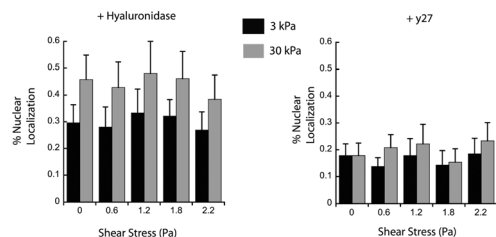


Fig. 7 NF- κ B translocation in response to post-shearing (5 h) TNF- α treatment for cells treated with hyaluronidase and y27, a ROCK inhibitor. Cells on both substrates did not exhibit a significant change in the inflammatory response over the range of shear stress levels used compared to static controls. The data was produced by 2 independent experiments and $24 < n < 29$.

Conclusions

The present study demonstrates that the response of endothelial cells to shear stress is modulated by the stiffness of the extracellular matrix to which they adhere. This finding is crucial for understanding the behaviour of endothelial cells inside stiffening arterial walls, which are characteristic of multiple pathologies and normal aging. We observed changes in cell morphology and alignment in response to fluid shear stress across varying magnitudes of substrate elastic modulus. More relevant to cardiovascular disease, we found that the shear-stimulated endothelial cell response to the inflammatory cytokine TNF- α depended on the stiffness of the substrate. These results followed the same, general trend: high stiffness substrates masked the response of the endothelial cells to a range of fluid shear stress magnitudes. On a soft substrate, cells respond differently to a 1.2 Pa shear stress compared to 2.2 Pa. A cell on a stiff substrate is unaffected by the same increase in shear stress, based on both morphological and inflammatory responses. These findings support *in vivo* data showing a correlation between arterial stiffness and the inflammatory and atherosclerotic response.⁴

Shear stress can affect the function of endothelial cells through the activation of mechanosensors, specific transcription factors, intracellular signalling pathways, and the expression of genes and proteins.^{32–35} The results of the present study suggest that substrate mechanics can modulate the effects of shear stress, which has obvious implications for atherosclerosis and other pathologies associated with vascular stiffening. It is difficult to ally the morphological results with *in vivo* physiology, especially since cells were tested at subconfluency. However, the ability of substrate stiffness to reduce the sensitivity of sheared endothelial cells to TNF- α suggests an additional means by which vascular stiffening is pro-inflammatory.

Elucidating the mechanisms underlying the stiffness-modulated response to shear stress is necessary to understand the biochemical pathways involved and subsequently manipulate them for therapeutic purposes. The abrogation of the response to shear stress with hyaluronidase and a hyaluronan synthase inhibitor suggests that the upstream mechanosensor is related to the glycocalyx, which has been previously identified as a sensor of shear stress.³⁶ Fluid shear stress has also been shown to increase the levels of hyaluronan in the glycocalyx,³⁷ suggesting the presence of a feedback loop that involves shear stress and hyaluronan and the glycocalyx. There is evidence in literature that several HA receptors have downstream effectors that are important regulators of the inflammatory response including CD44 and RHAMM.^{38,39}

The effects of substrate stiffness and shear stress on cell morphology, stiffness, and response to TNF- α are not monotonically related. For example, increased substrate stiffness in static conditions leads to increases in all three features, but on soft and intermediate stiffness substrates in the range of normal vasculature, imposition of apical shear stress

strongly increases cell alignment and stiffness, with a smaller effect on cell area, but it decreases the response to TNF- α . Some if not all of these responses can be altered by actomyosin-generated cell contraction, and a crucial regulator of contractility is the Rho-ROCK pathway. The ROCK inhibitor identified Rho as a potential mediator of the response to combined solid and fluid mechanical stimulation. CD44, an HA receptor that affects Rho/ROCK signalling could be the link between hyaluronan and Rho: shear deforms the hyaluronan-containing glycocalyx and activates CD44, which enhances Rho activation and induces spreading on soft substrates. Having a common downstream component, like Rho, could explain how substrate mechanics could saturate the pathway and subsequently mask the cell response to shear stress.

Future directions will involve investigating several cell mechanics phenomena in response to combined shear and substrate stimuli. For example, focal adhesion size and dynamics are known to be affected by substrate stiffness,^{40,41} and shear stress can activate FAK on endothelial cells plated on rigid substrates.⁴² The present device provides a platform to study the effect of these combined stimuli on the formation and duration of focal adhesions. A second direction is the role of nitric oxide secretion by the endothelial cells. Fluid shear stress is known to augment secretion of NO from the endothelium,⁴³ and studies in bone have demonstrated NO release is morphologically dependent.⁴⁴ The present device can be used to investigate the combined effects of flow and substrate stiffness on NO release.

Acknowledgements

This work was supported by from a T32 Interdisciplinary Cardiovascular Training Grant from the National Institutes of Health (to P.G.), a Fulbright Science and Technology award and a Kuitse Fund – Prins Bernhard Fund fellowship (to A.v.O.). P.G. thanks Juan Jimenez for use of his parallel shear device and to Peter Davies for helpful discussions.

Notes and references

- 1 S. Laurent, *J. Hypertens.*, 2012, **30**, S3–S8.
- 2 E. L. Schiffrin, A. Tedgui and S. Lehoux, *Blood Pressure and Arterial Wall Mechanics in Cardiovascular Diseases*, Springer, London, 2014, pp. 97–106.
- 3 A. D. Gepner, L. A. Colangelo, E. Hom, M. Tattersall, C. E. Korcarz, B. C. Astor, J. Kaufman, K. Liu and J. Stein, *J. Am. Coll. Cardiol.*, 2013, **61**, 10S.
- 4 D. Kothapalli, S. L. Liu, Y. H. Bae, J. Monslow, T. Xu, E. A. Hawthorne, F. J. Byfield, P. Castagnino, S. Rao, D. J. Rader, M. C. Phillips, S. Lund-Katz and R. K. Assoian, *Cell Rep.*, 2012, **2**(5), 1259–1271.
- 5 E. A. Klein, L. Yin, D. Kothapalli, P. Castagnino, F. J. Byfield, T. Xu, I. Levental, E. A. Hawthorne, P. A. Janmey and R. K. Assoian, *Curr. Biol.*, 2009, **19**(18), 1511–1518.
- 6 K. Kliche, P. Jeggle, H. Pavenstädt and H. Oberleithner, *Pfluegers Arch.*, 2011, **62**(2), 209–217.
- 7 A. J. Engler, S. Sen, H. L. Sweeney and D. E. Discher, *Cell*, 2006, **126**(4), 677–689.
- 8 D. E. Discher, P. A. Janmey and Y. L. Wang, *Science*, 2005, **310**(5751), 1139–1143.
- 9 V. Vogel and M. Sheetz, *Nat. Rev. Mol. Cell Biol.*, 2006, **7**(4), 265–275.
- 10 F. J. Byfield, R. K. Reen, T. P. Shentu, I. Levitan and K. J. Gooch, *J. Biomech.*, 2009, **42**(8), 1114–1119.
- 11 T. Yeung, P. C. Georges, L. A. Flanagan, B. Marg, M. Ortiz, M. Funaki, N. Zahir, W. Ming, V. Weaver and P. A. Janmey, *Cell Motil. Cytoskeleton*, 2005, **60**(1), 24–34.
- 12 C. A. Reinhart-King, M. Dembo and D. A. Hammer, *Biophys. J.*, 2008, **95**(12), 6044–6051.
- 13 A. A. Birukova, X. Tian, I. Cokic, Y. Beckham, M. L. Gardel and K. G. Birukov, *Microvasc. Res.*, 2013, **87**, 50–57.
- 14 K. M. Stroka and H. Aranda-Espinoza, *Blood*, 2011, **118**(6), 1632–1640.
- 15 L. Sorokin, *Nat. Rev. Immunol.*, 2010, **10**(10), 712–723.
- 16 C. Vlachopoulos, I. Dima, K. Aznaouridis, C. Vasiliadou, N. Ioakeimidis, C. Aggeli, M. Toutouza and C. Stefanadis, *Circulation*, 2005, **112**(14), 2193–2200.
- 17 K. M. Maki-Petaja, C. M. McEniery, S. S. Franklin and I. B. Wilkinson, *Blood Pressure and Arterial Wall Mechanics in Cardiovascular Diseases*, Springer, London, 2014, pp. 435–444.
- 18 C. F. Dewey, M. A. Gimbrone, P. F. Davies and S. R. Bussolari, *J. Biomech. Eng.*, 1981, **103**(3), 177–185.
- 19 G. P. Sorescu, M. Sykes, D. Weiss, M. O. Platt, A. Saha, J. Hwang, N. Boyd, Y. C. Boo, J. D. Vega, W. R. Taylor and H. Jo, *J. Biol. Chem.*, 2003, **278**(33), 31128–31135.
- 20 O. Traub and B. C. Berk, *Arterioscler., Thromb., Vasc. Biol.*, 1998, **18**, 677–685.
- 21 K. Glen, N. Luu, E. Ross, C. D. Buckley, G. Rainger, S. Egginton and G. B. Nash, *J. Cell. Physiol.*, 2012, **227**(6), 2710–2721.
- 22 J. Partridge, H. Carlsen, K. Enesa, H. Chaudhury, M. Zakkar, L. Luong, A. Kinderlerer, M. Johns, R. Blomhoff, J. C. Mason, D. O. Haskard and P. C. Evans, *FASEB J.*, 2007, **21**(13), 3553–3561.
- 23 Y. T. Shiu, S. Li, W. A. Marganski, S. Usami, M. A. Schwartz, Y. L. Wang, M. Dembo and S. Chien, *Biophys. J.*, 2004, **86**(4), 2558–2565.
- 24 D. E. Conway, M. T. Breckenridge, E. Hinde, E. Gratton, C. S. Chen and M. A. Schwartz, *Curr. Biol.*, 2013, **23**(11), 1024–1030.
- 25 R. H. Lam, Y. Sun, W. Chen and J. Fu, *Lab Chip*, 2012, **12**(10), 1865–1873.
- 26 L. H. Ting, J. R. Jahn, J. I. Jung, B. R. Shuman, S. Feghhi, S. J. Han, M. L. Rodriguez and N. J. Sniadecki, *Am. J. Physiol.*, 2012, **302**, H2220–H2229.
- 27 B. Wojciak-Stothard and A. J. Ridley, *J. Cell Biol.*, 2003, **161**(2), 429–439.
- 28 T. G. Papaioannou and C. Stefanadis, *Hell. J. Cardiol.*, 2005, **46**(1), 9–15.

- 29 M. Y. Pahakis, J. R. Kosky, R. O. Dull and J. M. Tarbell, *Biochem. Biophys. Res. Commun.*, 2007, **355**(1), 228–233.
- 30 B. M. Fu and J. M. Tarbell, *Wiley Interdiscip. Rev.: Syst. Biol. Med.*, 2013, **5**(3), 381–390.
- 31 A. Chopra, M. E. Murray, F. J. Byfield, M. G. Mendez, R. Halleluyan, D. J. Restle, D. Raz-Ben Aroush, P. A. Galie, K. Pogoda, R. Bucki, C. Marcinkiewicz, G. D. Prestwich, R. J. Zarembinski, C. S. Chen, E. Pure, J. Y. Kresh and P. A. Janmey, *Biomaterials*, 2014, **35**(1), 71–82.
- 32 K. D. Chen, Y. S. Li, M. Kim, S. Li, S. Yuan, S. Chien and J. Y. Shyy, *J. Biol. Chem.*, 1999, **274**(26), 18393–18400.
- 33 S. Jalali, Y. S. Li, M. Sotoudeh, S. Yuan, S. Li, S. Chien and J. Y. Shyy, *Arterioscler., Thromb., Vasc. Biol.*, 1998, **18**(2), 227–234.
- 34 S. Jalali, M. A. del Pozo, K. D. Chen, H. Miao, Y. S. Li, M. A. Schwartz, J. Y. Shyy and S. Chien, *Proc. Natl. Acad. Sci. U. S. A.*, 2001, **98**(3), 1042–1046.
- 35 S. J. White, E. M. Hayes, S. Lehoux, J. Y. Jeremy, A. J. Horrevoets and A. C. Newby, *J. Cell. Physiol.*, 2011, **226**(11), 2841–2848.
- 36 S. Weinbaum, X. Zhang, Y. Han, H. Vink and S. C. Cowin, *Proc. Natl. Acad. Sci. U. S. A.*, 2003, **100**(13), 7988–7995.
- 37 M. Gouverneur, J. A. Spaan, H. Pannekoek, R. D. Fontijn and H. Vink, *Am. J. Physiol.: Heart Circ. Physiol.*, 2006, **59**(1), H458.
- 38 C. Tolg, S. R. Hamilton, E. Zalinska, L. McCulloch, R. Amin, N. Akentieva, F. Winnik, R. Savani, D. J. Bagli, L. G. Luyt, M. K. Cowman, J. B. McCarthy and E. A. Turley, *Am. J. Pathol.*, 2012, **181**(4), 1250–1270.
- 39 P. W. Noble, J. Liang and D. Jiang, *Physiol. Rev.*, 2011, **91**(1), 221–264.
- 40 R. J. Pelham and Y. Wang, *Proc. Natl. Acad. Sci. U. S. A.*, 1997, **94**(25), 13661–13665.
- 41 C. Grashoff, B. D. Hoffman, M. D. Brenner, R. Zhou, M. Parsons, M. T. Yang, M. A. McLean and M. A. Schwartz, *Nature*, 2010, **466**(7303), 263–266.
- 42 S. Li, M. Kim, Y. L. Hu, S. Jalali, D. D. Schlaepfer, T. Hunter, S. Chien and J. Y. Shyy, *J. Biol. Chem.*, 1997, **272**(48), 30455–30462.
- 43 G. M. Buga, M. E. Gold, J. M. Fukuto and L. J. Ignarro, *Hypertension*, 1991, **17**(2), 187–193.
- 44 R. G. Bacabac, D. Mizuno, C. F. Schmidt, F. C. MacKintosh, J. J. Van Loon, J. Klein-Nulend and T. H. Smit, *J. Biomech.*, 2008, **41**(7), 1590–1598.